A numerical study of vortex interactions for high- kappa superconductors

1994 J. Phys.: Condens. Matter 6 7373

(http://iopscience.iop.org/0953-8984/6/36/019)

J. Phys.: Condens. Matter 6 (1994) 7373–7384. Printed in the UK

A numerical study of vortex interactions for high-κ superconductors

S Aktas, C P Poole Jr and H A Farach

Department of Physics and Astronomy, University of South Carolina, Columbia, SC 29208, USA

Received 20 July 1993, in final form 22 February 1994

Abstract. The repulsive Lorentz force between two vortices in high-κ superconductors with the vortices aligned along the direction of axial symmetry was calculated by approximating the numerical integral by a set of polynomials to speed up the computations. Calculations were carried out to simulate formation of hexagonal vortex lattice from a population of 400 initially randomly distributed vortices. Small domains with different alignments of vortices were found at the early stages, and a single large domain with hexagonal order aligned with the edges emerged at the end. Also, the expansion of a vortex population was simulated and it kept its initial shape while it expanded isotopically outward into a larger area. The force exerted on a displaced vortex in an otherwise perfect lattice was calculated and it was found to be about the same order of magnitude as the force between two isolated vortices, and about ten times stronger than the force exerted on an extra interstitial vortex.

1. Introduction

One of the main problems that holds up the development of material high-temperature superconductors is the necessity to acquire a more complete understanding of the dynamics of flux lattice motion. Such motion involves the motion of individual vortices acting under the influence of strong forces from nearby vortices and weaker forces from more distant vortices. Pinning centres exert forces which can hold vortices in place, and the presence of transport current adds an additional force. The application of an applied magnetic field causes vortices to move into the superconductor. Vortices in motion also experience magnus forces and frictional drag forces. A proper understanding of how non-equilibrium vortex configurations evolve toward configurations that are in equilibrium with the internal and external forces can lead to the development of critical current enhancement techniques.

In the present article we will study the motion of an initial random distribution of vortices as they rearrange themselves into a final close-to-equilibrium configuration of a hexadic type. We will also investigate the force on a vortex displaced from its equilibrium position on an otherwise perfect hexadic lattice, and the force on an extra vortex at an arbitrary interstitial location in a perfect hexadic lattice.

2. Vortex arrays

At the lower critical field H_{c1}, an applied magnetic field starts to penetrate a type-II superconductor in the form of quantized magnetic vortices [1] carrying a quantum of flux Φ_0. A vortex consists of a normal-like region called the core with a radius equal to the

0953-8984/94/367373+12$19.50

coherence length ξ, and a region of circulating screening current J with a radius equal to the penetration depth λ. When the density of vortices is so low that their average separation is much larger than λ, the forces between them can easily be calculated through the Lorentz force expression, $F = J \times \Phi_0$, since the currents of one vortex can be assumed uniform over the region of the other vortex [2]. When the density of vortices increases to a point where the average distance between them is comparable with λ, then the force can no longer be calculated in this simple way, so the integral of $J \times B$ must be evaluated.

In this paper, first the Lorentz force was evaluated through the numerical integration of $J \times B$, and then this integral was replaced by a polynomial approximation to shorten the computer time. The formation of a hexagonal vortex lattice was simulated starting with a random population of 400 vortices. Then the expansion of a random vortex area into a larger area was simulated. In the last section, the force exerted on a displaced and on an interstitial vortex in an otherwise perfect hexagonal vortex lattice was studied.

3. Lorentz force between two vortices

The London equations can be used to treat the vortices up to the density where they have the separation $D \approx 5.4\xi$ [3,4] which corresponds to an applied field of about $\frac{1}{4}H_{c2}$ for $\kappa = \lambda/\xi = 100$. This approach is especially appropriate for high-κ cases such as the cuprates, where the core region can be treated as point-like compared with the penetration depth λ.

The field and the current distributions of a single vortex obtained by solving the London equations in an isotropic plane are given by [5,6]

$$B(r) = \frac{\Phi_0}{2\pi\lambda^2} K_0(r/\lambda) \tag{1}$$

$$J(r) = \frac{\Phi_0}{2\pi\mu_0\lambda^3} K_1(r/\lambda) \tag{2}$$

where $K_0(r/\lambda)$ and $K_1(r/\lambda)$ are zeroth- and first-order modified Bessel functions, respectively. The vortices are assumed to be aligned with the symmetry of the axially symmetric superconductor.

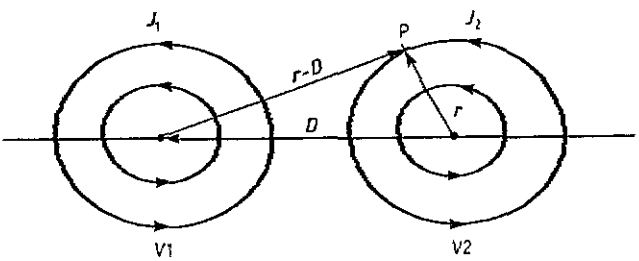

Figure 1. Position coordinates used for the calculation of the Lorentz force between two vortices by integration. J_1 and J_2 are circulating supercurrents of vortices v1 and v2.

Using the field and the current distributions given by equations (1) and (2), the differential force density $\mathrm{d}f(r)$ exerted at the point P in figure 1 on the screening current of vortex v2 by the field of the vortex v1 is given by

$$\mathrm{d}f(r) = \mathrm{d}J_2(r) \times B_1(|r - D|) \tag{3}$$

where D is the separation of the two vortices. The force on the whole current ring of radius r is then the integral of $df(r)$ over the ring. Another integral over the rings with different radii gives the total force per unit length $F(D)$ exerted on the vortex v2 by the vortex v1. Since we are not interested in the length of the vortices we will call $F(D)$ simply the force between vortices. This Lorentz force is along the line that connects the two vortices, and is repulsive. Figure 2 shows this force $F(D)$ calculated as a function of their separation. The plot is normalized to a value close to 1 at its maximum point, and this normalization condition is used for the rest of the paper.

The force $F(D)$ goes to zero as the separation D goes to zero at the total overlap of vortices. It must, however, be remembered that the superconductivity is lost when the average separation becomes comparable with the coherence length. The repulsive force reaches its maximum at about $D = 0.5\lambda$.

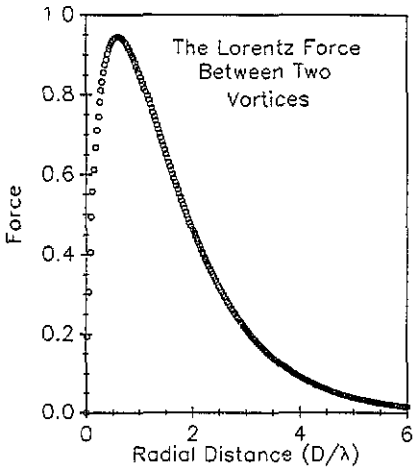

Figure 2. Dependence of the force between two vortices on their separation D. The force is normalized to 0.95 at the maximum, and the separation is normalized to the penetration depth λ.

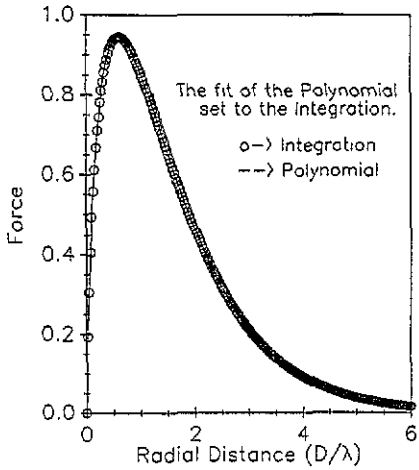

Figure 3. Polynomial fit (——) to the calculated force points (O) of figure 2.

The numerical integral calculations take about 1–2 s of CPU time per pair of vortices. When many vortices are present, the force F on a particular vortex at position r_0 is the vector sum of the forces $F_1(r_1 - r_0)$ exerted on it by all the other vortices. Computations involving many vortices can be limited by the available computer time. For example a simulation involving 400 vortices requires 160 000 force calculations for a single step toward determining the total forces on all the vortices, and this can add up to 50 or more hours of CPU time. Using a linear regressional fit, a set of polynomials was fitted to the force curve of figure 2. This considerably reduces the computer time, and the result plotted in figure 3 shows the excellent agreement between the actual integration and the polynomial approximation for the range $0 < D < 6\lambda$.

4. Simulations of a vortex lattice

The repulsive Lorentz force causes the vortices to average themselves on a triangular lattice to their lowest-energy state. The formation of this vortex lattice is studied by calculations

which involve the determination of the force on an individual vortex arising from the vector sum of the forces from each of the remaining 399 vortices. The magnitude of each such individual force is obtained from the polynomial approximation. After obtaining this net force the vortex is moved a distance Δr in the direction of this force, with all of the other vortices held in place.

Vortices near the edge of the superconductor experience an additional surface force from the applied external field which prevents them from leaving the material. This surface repulsive force is assumed to decay exponentially with distance from the surface to the inside. Thus a vortex a distance d from the edge experiences the force $F_0 e^{-d/\lambda}$ acting away from the edge. The value of F_0 was found by trial and error such that the vortices are held inside the superconducting material within one penetration depth λ of the edge.

The net force acting on each vortex is thus the sum of the Lorentz forces from the other 399 vortices plus the sum of the forces from the four edges of the square region containing the vortices. Since the vortex motion involves displacements Δr that are determined by this net force there is no equation of motion needed to describe the displacements. The vortices remain fixed in position between iterations, and only one vortex is displaced at a time.

To start with the simulation, 400 random vortices are put in a square with sides equal to 40 λ. One vortex is selected and the vector force on it due to the remaining 399 vortices plus that from the four edges is calculated. The vortex is then moved a distance $\Delta r = 0.1\lambda$ in the direction of this force. This process is then repeated for the remaining 399 vortices. The resulting change in vortex configuration from the initial random one is called a move. The whole process itself is repeated until the effect of further iterations becomes negligible. After every 10 or 20 moves the distance of the displacement Δr is decreased until it becomes 0.01λ for the final 300 moves.

Figure 4 shows the initial random vortex distribution. Figures 4(b) to 4(d) display the evolution toward a hexagonal arrangement. Figure 4(b) exhibits the beginning of triangular short-range order in the centre and linear alignment along the edges after 50 moves. Then 400 moves later we see from figure 4(c) that the hexagons are more regular, those near edges tend to align with edges, and centrally located vortices tend to align with the left and right edges. At the corners, vortices tend to form square patterns in order to comply with the corner geometry. At this stage there are not many regular hexagons. Figure 4(d) confirms the left–right edge alignment which covers most of the square with a regular hexagonal order after 2000 moves.

Thus from the beginning, the edge effect is a dominant factor in determining the final alignment of hexagons. In order to minimize the edge effect, an initial random vortex distribution was established in a $20\lambda \times 20\lambda$ square region at the centre of a $40\lambda \times 40\lambda$ square away from the edges. This reduces the influence of edges on the vortices at the early stages of the iteration. Figure 5(a) shows the initial random arrangement. After 50 moves, figure 5(b) displays the outward advancement of the vortex region. Apart from expanding outward, the vortices reach a fairly uniform distribution among themselves with the beginnings of hexagonal order, and they start to pile up at the boundary while the boundary keeps its square shape. After 400 moves, figure 5(c) displays the growth of the hexagonally ordered central domain in which the hexagons are not aligned with the edges. The vortices pile up along edges and at corners. Figure 5(d) after 2000 moves shows that the central domain grows to a larger area and becomes more regular while it still does not align with the edges. The pre-established hexagonal order in the centre is relatively stable against the edge effect.

When the final pictures of these two different simulations are examined, we see that the long-range hexagonal order is broken at the boundaries of domains where there are

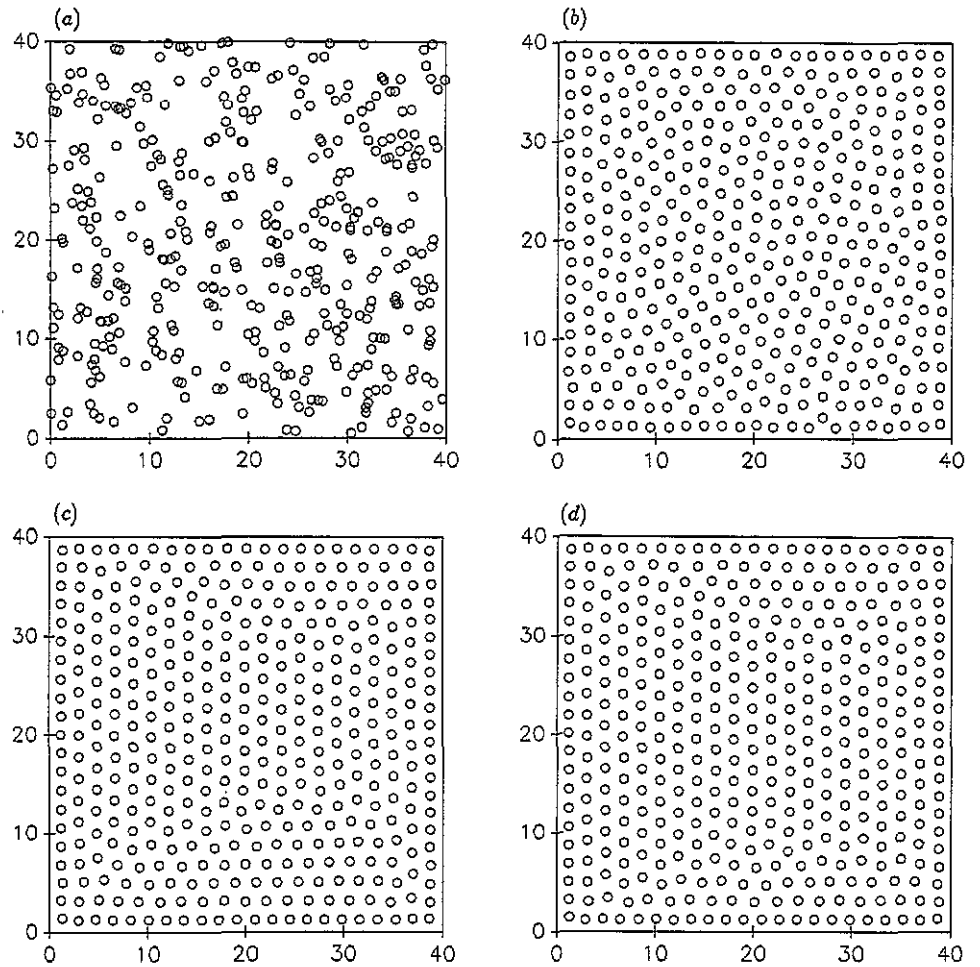

Figure 4. Plots of positions of 400 vortices on $40\lambda \times 40\lambda$ square. (a) Initial random arrangement, (b) 50 moves later, (c) after 400 moves, and (d) after 2000 moves.

deformed hexagons. A deformed hexagon of a simplest type has a displaced vortex or an extra (interstitial) vortex within an hexagonal unit. By examining the force exerted on these 'improperly located' vortices, we may get an insight on the strength of a possible pinning which may lead to similar kinds of deformed hexagons.

5. Defects in a vortex lattice

The simplest case to treat is that of one improperly located vortex in an otherwise perfect hexagonal vortex lattice. Although this may represent an oversimplification, it could give us some basic insights on the behaviour of defects. Two cases were treated; (a) a displaced vortex, and (b) an interstitial vortex.

(a) *Displaced vortex.* The triangular vortex lattice was viewed from a central lattice point with surrounding hexagonal vortex rings. The displacement of the vortex at this point was studied by assuming that all the other vortices in the lattice are held at their proper

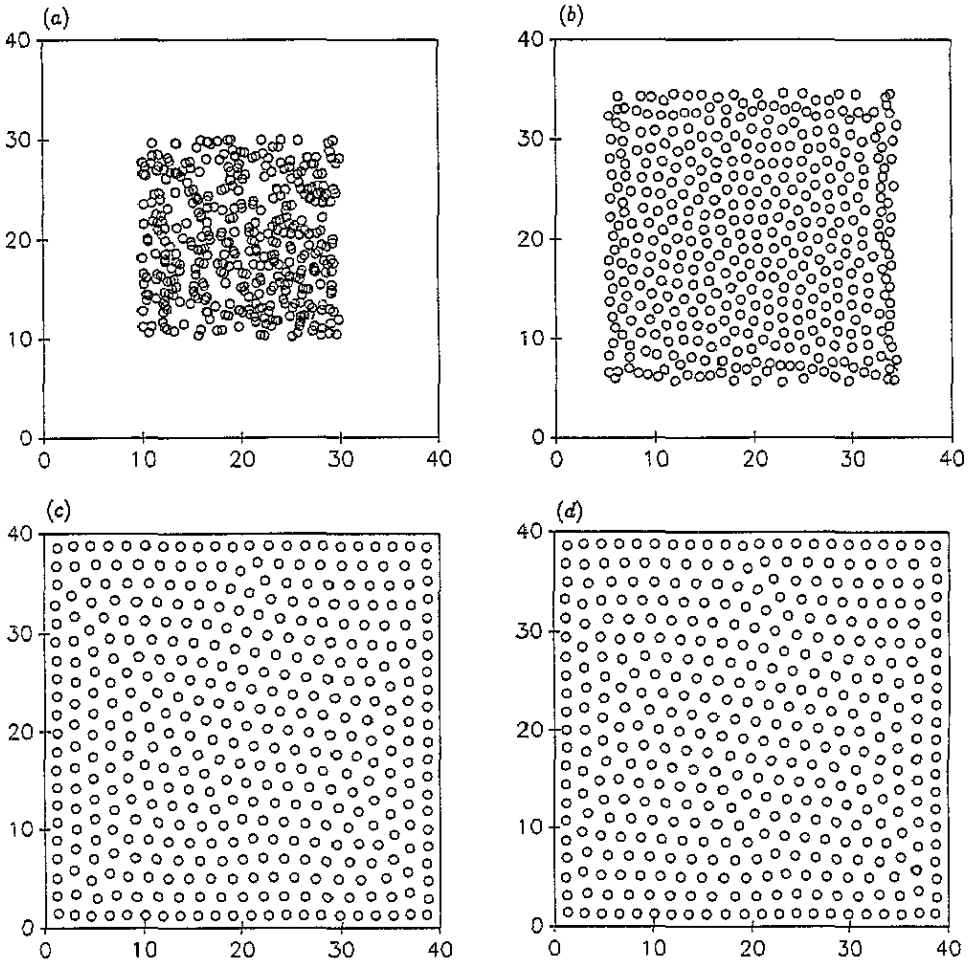

Figure 5. Plots of positions of 400 vortices placed initially in a $20\lambda \times 20\lambda$ square centred inside a $40\lambda \times 40\lambda$ square. (a) Initial random position, (b) expansion after 50 moves, (c) after 400 moves, and (d) configuration after 2000 moves.

hexagonal sites. The displacement was specified by a radial distance r, and angle ϕ as seen in figure 6. The total force on this displaced vortex was calculated for a series of angles ϕ, and radial displacements r. Figure 7 shows the radial dependence of the force exerted on the displaced vortex where two extreme cases of angles ($\phi = 0°$ and $\phi = 30°$) were plotted. It is sufficient to cover the angular range of $0° < \phi < 30°$ because of the 12-fold symmetry. The force rises linearly for both angles when the displacement r is small, and it is always directed toward the centre of the hexagon (the angles of the force are not shown in the figure). This resembles the restoring force of a spring. We see from figure 8 that the force is greater for $D = \lambda$ than it is for $D = \frac{1}{2}\lambda$ and $D = 2\lambda$ but the change in magnitude is small.

(b) *Interstitial vortex.* Another possible type of defect is having an extra vortex inserted at an interstitial position in the lattice. The same kind of calculation was repeated for this case, and the results are plotted in figure 9 for three angles $\phi = 0°$, 15°, 30°. The $\phi = 0$ line goes from vortex v to v′ through the saddle points, the $\phi = 30°$ line goes from vortex v

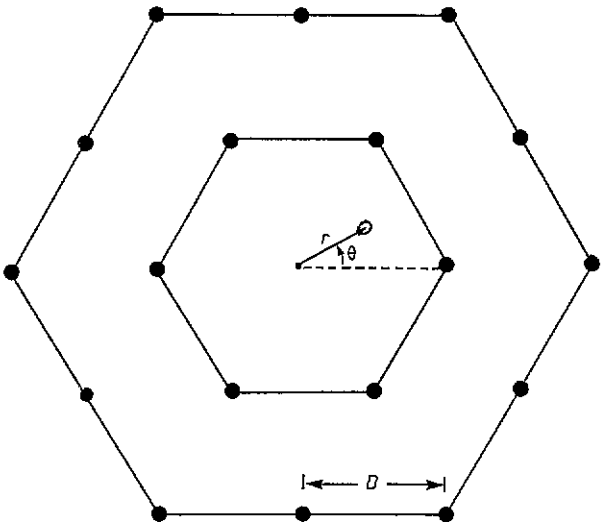

Figure 6. Vortex (designated by a hollow circle) shown displaced at the position, (r, θ) from the centre of the regular hexagon. D is the separation of vortices in the lattice.

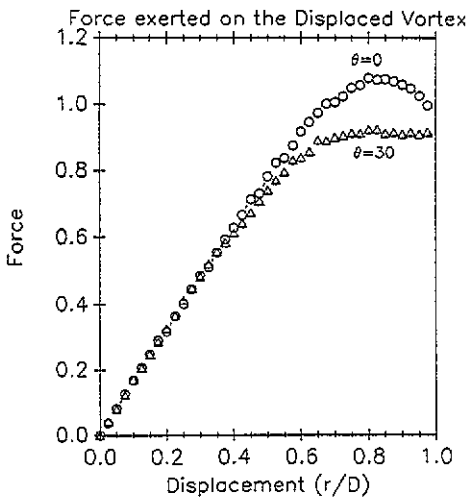

Figure 7. Dependence of the force exerted on the displaced vortex of figure 6, on the radial displacement r. The circles are for radial displacements at the angle $\theta = 0°$, and the triangles for displacements at the angle $\theta = 30°$.

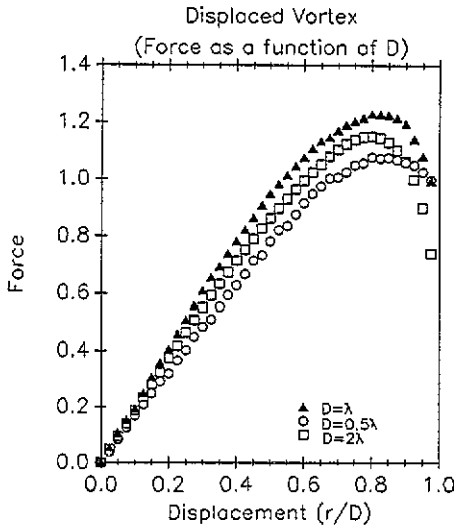

Figure 8. Dependence of the force on the displaced vortex of figure 6 on the radial displacement r at the angle $\theta = 0°$ for three lattice separations $D/\lambda = 1/2$, 1, 2.

through the midpoint M and then through the saddle point S′, using the notation of figure 10. There are two equilibrium positions shown by the points S, S′ and M for such an interstitial vortex. The centre point M of the triangle on figure 10 is the only stable location for the interstitial vortex. The saddle point S at the midpoint on the line between two vortices is highly unstable for displacements off this line.

The saddle point S is the distance $r = \frac{1}{2}D$ and the centre point M is at the distance

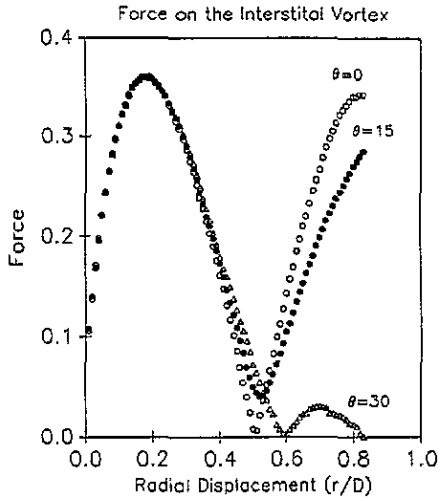

Figure 9. Dependence of the force on an interstitial vortex on its radial position r relative to vortex V of figure 10 for three different angles. The angle $\theta = 0$ corresponds to the line V–S–V′ and $\theta = 30°$ corresponds to the line V–M–S′ of figure 10.

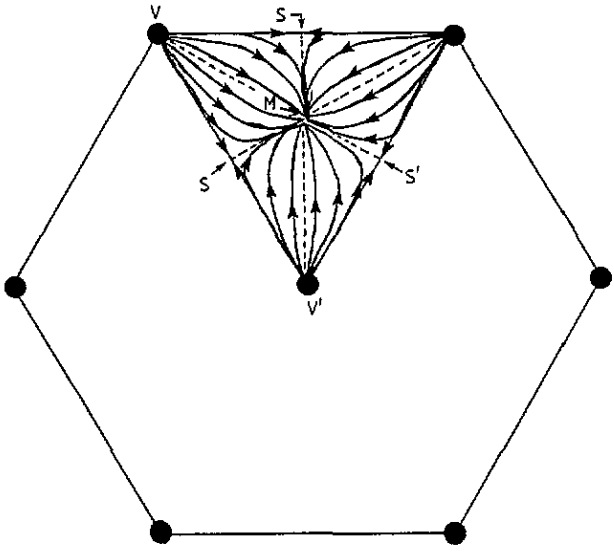

Figure 10. Sketch of the force lines involving an interstitial vortex. The calculations use a coordinate system with V at the origin, with the line V–S–V′ corresponding to $D = 0$, and V–M–S′ corresponding to $\theta = 30°$.

$r = D/\sqrt{3}$ from the vortex v, and within the range $0.5 < (r/D) < 1/\sqrt{3}$ the magnitude of the force for each angle goes through a minimum. In addition, within this range the curves cross over and reverse their order in terms of magnitude. Detailed calculations were carried out for this range of r/D, and the results shown in figure 11 reveal that the force exerted on the interstitial vortex increases monotonically for fixed radial displacements of $r = 0.46$ and $r = 0.5$ for increasing angle, while it stays almost constant for $r = 0.54$. The next

two cases of $r = 0.58$ and $r = 0.62$ show the opposite behaviour with the force decreasing monotonically for increasing angle.

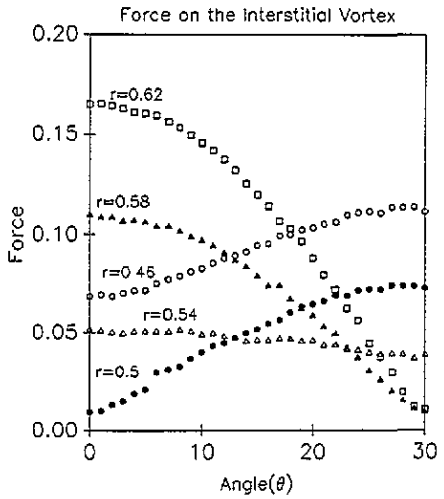

Figure 11. Dependence of the force exerted on the radial displacement r of an interstitial vortex at the angle $\theta = 30°$ for three lattice separations D/λ = 1/2, 1, 2.

We note from figure 10 that over this region of distance the force is toward the central point M, pointing in a direction almost perpendicular to the line V–S–V.

Force calculations were carried out for the angle $\phi = 30°$ with the three vortex separations D/λ = 1/2, 1 and 2. The results presented in figure 12 show that the separation of vortices strongly affects the magnitude of the force as shown in figure 12, unlike the former case of a displaced vortex in figure 9 where the magnitude of the force only changes slightly.

6. Discussion

It was found that during the first simulation, small domains with different alignments appear and grow as has been observed in decoration experiments [8–12]. Eventually, one of the domains aligned with an edge engulfs others and proceeds to extend throughout the vortex population. The edges were a dominant factor in determining the alignment of the hexagons. Such surface effects have been reported by others [13–15].

In the second simulation, the initial random vortices were placed away from edges so that at the early stages of the simulation the rearrangements were not influenced by the edges. The final arbitrary alignment of the large central domain shows the stability and cohesiveness of a well formed hexagonal region. During early stages of expansion the vortex region retained its initial square shape while the vortex population expanded isotopically outward into the larger square.

The 400 vortices that were selected for carrying out the simulations is typical of the number that might be in one grain of a high-temperature superconductor. This may be shown by equating the total flux BA in a grain of cross sectional area A to the number

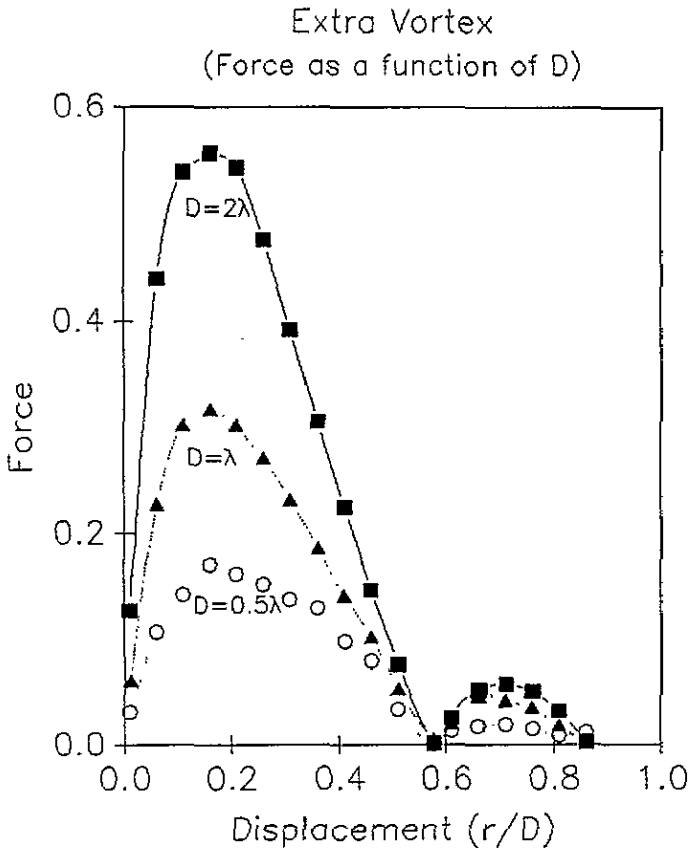

Figure 12. Force dependence on the radial displacement r of an interstitial vortex at the angle $\theta = 30°$ for three lattice separations $D/\lambda = 1/2, 1, 2$.

of fluxons N times the quantum of flux $\Phi_0 = 2.0679 \times 10^{-15} TM^2$, and this gives for the internal magnetic field B_{in} within the grain

$$B_{in} = n\Phi_0/A. \tag{4}$$

Therefore a typical superconducting grain of area 1 μm^2 containing $N = 400$ vortices will have an internal field of 0.8 T. The externally applied field B_{app} that produces this internal field will be larger than 0.8 T because (a) the superconductor has a negative susceptibility, and (b) the typical high-temperature superconductor penetration depth of 0.1 μm causes the effective area of superconducting material inside the penetration depth to be only about 2/3 of the actual area. Thus the number of vortices chosen for the simulations was typical of that in a high-superconductor grain. Simulations representative of much larger grain sizes or much larger applied fields could be carried out using periodic boundary conditions [16].

The calculations of the force exerted on an improperly positioned vortex on a regular hexagonal lattice reveal that it is the same order of magnitude as the force between two isolated vortices, and about ten times larger than the force on an interstitial vortex. Therefore any pinning force which may cause this type of displacement must be as strong as this calculated force for it to pin down the vortex at such a position.

The simulation technique that we used does not take into account the possibility of different vortex phases such as the liquid or glassy state, or the refinements of flux lattice

melting and flux creep. These phenomena only occur at finite temperatures, and so cannot be simulated by a method which takes no account of thermal effects. Pinning centres could be included in the simulations, but no attempt was made to do so.

In the present work we have calculated the configuration for $T = 0$. Typically, at temperatures different from zero, the excited state configurations involving fluctuations in vortex positions 16–23 occur with probabilities that depend on the energy and the temperature. We only keep configurations that minimize the force corresponding to the minimum ground state for $T = 0$. The force calculations between vortices do not give the energy change of different vortex configurations in a simple way. In order to include the temperature effect, it is necessary to evaluate the total energy of the system of vortices each time a move is made, and this would require an enormous amount of computer time. Simulations for $T > 0$ are more appropriately carried out using Monte Carlo techniques [24, 25] that will be commented upon below.

If thermal effects were taken into account then higher temperatures would involve a slower approach to equilibrium and a final equilibrium state, and this final state would have some vortices displaced from their regular hexadic positions due to thermal fluctuations. The regular hexadic arrangement is the equilibrium configuration for $T = 0$. Vortex lattice melting [26–29] and flux creep [30–34], which occur at finite temperatures, could not be taken into account. Recent articles discuss models, calculations and simulations of lattice melting [35–40] and flux creep [41–45].

Other approaches have been employed to carry out calculations of vortex lattices [46]. The Lorentz equations have been employed to simulate the lattice [47], and a number of Monte Carlo simulations [44, 45, 48, 49] have been published. These articles do not report the type of data that were presented here, so our results are not directly comparable with theirs. The Monte Carlo technique has the advantage of being based on energy calculations, so it permits the determination of the specific heat [39, 48] which is not readily found by the force calculation method.

References

[1] Abrikosov A A 1957 *Zh. Eksp. Teor. Phys.* **32** 1442
[2] Tinkham M 1985 *Introduction to Superconductivity* (Malabar, FL: R E Krieger)
[3] Brandt E H 1972 *Phys. Status Solidi* b **51** 345
[4] Brandt E H 1988 *Phys. Rev.* B **37** 2349
[5] Orlando T P and Delin K A 1991 *Foundations of Applied Superconductivity* (Reading, MA: Addison-Wesley)
[6] Poole C P Jr, Farach H A and Creswick R 1994 *Textbook of Superconductivity* (Boston, MA: Academic) at press
[7] Essmann U and Trauble H 1967 *Phys. Lett.* **24A** 52
[8] Kleiman R N, Broholm C, Aeppli G, Bucher E, Stücheli N, Bishop N J, Clausen K N, Mortensen K, Pedersen J S and Howard B 1992 *Phys. Rev. Lett.* **69** 3120
[9] Dolan G J, Chandrashekhar G V, Dinger T R, Feild C and Holtzberg F 1989 *Phys. Rev. Lett.* **62** 827
[10] Muller H, Suenaga M and Yokoyama Y 1991 *J. Appl. Phys.* **70** 4409
[11] Vinnikov L Ya and Grigor'eva I V 1988 *JETP Lett.* **47** 106
[12] Yethiraj M, Mook H A, Wignall G D, Cubitt R, Fogan E M, Paul D M and Armstrong T 1993 *Phys. Rev. Lett.* **70** 857
[13] Huse D H 1992 *Phys. Rev.* B **46** 8621
[14] Glatzer D, Forkl A, Theuss H, Habermeier H U and Kronmüller H 1992 *Phys. Status Solidi* b **170** 549
[15] Mohamed M A-K, Jung J and Franck J P 1989 *Phys. Rev.* B **39** 9614; 1990 *Phys. Rev.* B **41** 6406
[16] Doria M M, Gubernatis J E and Rainer D 1989 *Phys. Rev.* B **39** 9573
[17] Brandt E H 1989 *Physica* C **162** 1167
[18] Brandt E H 1989 *Phys. Rev. Lett.* **63** 1106
[19] Koka S and Shrivastava K N 1990 *Physica* B **165, 166** 1097

[20] Koko S and Shrivastava K N 1990 *Solid State Commun.* **75** 911
[21] Kogan V G, Ledvij M, Simonov A Yu, Cho J H and Johnston D C 1993 *Phys. Rev. Lett.* **70** 1870
[22] Nelson D R 1989 *J. Stat. Phys.* **57** 511
[23] Zuo F, Vacaru D, Duan H M and Hermann A M 1992 *Phys. Rev.* B **47** 8327
[24] Minnhagen P and Weber H 1985 *Phys. Rev.* B **32** 3337
[25] Weber H and Minnhagen P 1988 *Phys. Rev.* B **38** 8730
[26] Kwok W K, Fleshler S, Welp U, Vinokur V M, Downey J, Crabtree G W and Miller M M 1992 *Phys. Rev. Lett.* **69** 3770
[27] Safar H, Gammel P L, Huse D A, Bishop D J, Rice J P and Ginsberg D M 1992 *Phys. Rev. Lett.* **69** 824
[28] Worthington T K, Fisher M P A, Huse D A, Toner J J, Marwick A D, Zabel T, Feild C A and Holtzberg F 1992 *Phys. Rev.* B **46** 11 845
[29] Yeh N-C, Reed D S, Jiang W, Kirplani U, Holtzberg F, Gupta A, Hung B D, Vasquez R P, Foote M C and Bajuk L 1992 *Phys. Rev.* B **45** 5654
[30] Campbell I A, Fruchter L and Cabanel R 1990 *Phys. Rev. Lett.* **64** 1561
[31] Ossandon J G, Thompson J R, Christen D K, Sales B C, Sun Y and Lay K W 1992 *Phys. Rev.* B **46** 3050
[32] Zhao B-r, Kuroumaru S-i, Horie Y, Yanada E, Aomine T, Qiu X-g, Zhang Y-z, Zhao Y-y, Xu P, Li L, Ohkubo H and Mase S 1991 *Physica* C **138** 409
[33] Zuo F, Salamon M B, Datta T, Ghiron K, Duan H and Hermann A M 1991 *Physica* C **176** 541
[34] Pencarinha J, Poole C P Jr and Farach H A 1994 *Phys. Rev.* B submitted
[35] Brass A and Jensen H J 1989 *Phys. Rev.* B **39** 9587
[36] Hetzel R E, Suboø A and Huse D A 1992 *Phys. Rev. Lett.* **69** 518
[37] Jensen H J, Brass S, Shi A-c and Berlinsky A J 1990 *Phys. Rev.* B **41** 6394
[38] Sengupta S, Dasgupta C, Krishnamurthy H R, Menon G I and Ramakrishnan T V 1991 *Phys. Rev. Lett.* **67** 444
[39] Li Y-H and Teitel S 1991 *Phys. Rev. Lett.* **66** 3301
[40] Ryu S, Doniach S, Deutscher G and Kapitulnik A 1992 *Phys. Rev. Lett.* **68** 710
[41] Fischer K H and Nattermann T 1991 *Phys. Rev.* B **43** 10 372
[42] Mee C, Rae A I M, Vinen W F and Gough C E 1991 *Phys. Rev.* B **43** 946
[43] Xenikos D G and Lemberger T R 1990 *Phys. Rev.* B **41** 869
[44] Chakravarty S, Ivlev B I and Ovchinnikov Yu N 1990 *Phys. Rev.* B **42** 2143
[45] Rae A I M 1991 *Phys. Rev.* B **43** 2956
[46] Klein U 1987 *J. Low Temp. Phys.* **69**
[47] Daemen L I and Bubernatis J E 1991 *Phys. Rev.* B **43** 413
[48] Carnero G, Cavalcanti R and Gartner A 1992 *Phys. Rev.* B **47** 5263
[49] Ma H-r and Chui S T 1992 *Phys. Rev. Lett.* **68** 2428